A Direct Reconstruction Algorithm for Electrical Impedance Tomography

Jennifer L. Mueller*, Samuli Siltanen, and David Isaacson

***Abstract*—A direct (noniterative) reconstruction algorithm for electrical impedance tomography in the two-dimensional (2-D), cross-sectional geometry is reviewed. New results of a reconstruction of a numerically simulated phantom chest are presented. The algorithm is based on the mathematical uniqueness proof by A. I. Nachman [1996] for the 2-D inverse conductivity problem. In this geometry, several of the clinical applications include monitoring heart and lung function, diagnosis of pulmonary embolus, diagnosis of pulmonary edema, monitoring for internal bleeding, and the early detection of breast cancer.**

***Index Terms*—Dbar method, direct reconstruction algorithm, electrical impedance tomography.**

I. Introduction

In this paper we review a direct reconstruction algorithm for the electrical impedance tomography (EIT) problem in the two-dimensional (2-D) , cross-sectional geometry and present new results of a reconstruction of a numerically simulated phantom chest. In this geometry, several of the clinical applications include monitoring heart and lung function, diagnosis of pulmonary embolus, diagnosis of pulmonary edema, monitoring for internal bleeding, and the early detection of breast cancer.

The first implementation of the direct reconstruction algorithm was published in [27] and was tested on smooth, radially symmetric conductivity distributions. This method is very different from previous EIT algorithms in that it is noniterative and is based on a mathematical proof by A. Nachman [25] that uses the $\bar{\partial}$ method of inverse scattering to prove global uniqueness for the 2-D inverse conductivity problem. Nachman's solution method is remarkable since it reduces the nonlinear reconstruction problem to solving two linear integral equations. In [27], we present the first implementation of Nachman's algorithm. In [29], we extend our implementation to slightly more complicated radially symmetric conductivities. In [24], we consider several nonsymmetric examples and develop a regularization technique to handle the ill posedness in the problem as it manifests itself in this algorithm.

We briefly review existing reconstruction algorithms for EIT. To date, existing algorithms can be sorted into the following three categories:

1) noniterative linearization-based algorithms;
2) iterative algorithms solving the full nonlinear problem;
3) layer-stripping algorithms.

Linearization algorithms are based on the premise that the conductivity differs only slightly from a known, often constant, conductivity. Examples of linearization-based algorithms include backprojection methods [4], [6], [26], Calderón's approach [10], [11], [16], moment methods [1], and one-step Newton methods [7], [12], [22], [23]. However, the basic premise that the conductivity variations are small is often incorrect in physiological applications, such as the detection of breast tumors, which are known to be two to four times more conductive than healthy breast tissue [31], [32].

Algorithms solving the full nonlinear problem have been iterative in nature, with the exception of layer-stripping [30], [33]. These iterative algorithms have been based on output least-squares [8], [9], [13], [14], [15], [18], [19], [35], the equation-error formulation [20], [21], [34], or statistical inversion [17]. While these approaches are promising for obtaining accurate reconstructed conductivity values, they may be slow to converge.

The direct method reviewed in this paper represents a new class of algorithms for EIT. It solves the full nonlinear problem, so it has the potential of reconstructing the conductivity values with high accuracy.

The paper is organized as follows. In Section II, we state the equations governing the physical problem. In Section III we describe the steps of the reconstruction algorithm. In Section IV, we describe the numerical methods used in implementing the algorithm. Section V contains a numerical example with a numerically simulated phantom chest.

II. The Mathematical Model

The electromagnetic field induced by applying a current density to the surface of the body is governed by Maxwell's equations. At low frequencies and small field strengths the electromagnetic properties of living tissue allow these to be simplified to the conductivity equation

$$\nabla \cdot (\gamma(x,y)\nabla u(x,y)) = 0, \quad (x,y) \in \Omega. \tag{1}$$

Here, Ω denotes a bounded region in the plane, γ denotes the conductivity of the body, and u the electric potential. Applying

Manuscript received October 17, 2001; revised April 9, 2002. This work was supported in part by the Center for Subsurface Sensing and Imaging Systems (Cen SSIS) through the Engineering Research Centers Program of the National Science Foundation (NSF) under Award EEC-9986821. The work of J. L. Mueller was supported in part by the NSF under Grant DMS-0104861. *Asterisk indicates corresponding author.*

*J. L. Mueller is with the Colorado State University, Fort Collins, CO 80523 USA (e-mail: mueller@math.colostate.edu).

S. Siltanen is with the Instrumentarium Corporation, Imaging Division, FIN-04301 Tuusula, Finland.

D. Isaacson is with the Rensselaer Polytechnic Institute, Troy, NY 12180 USA.

Publisher Item Identifier 10.1109/TMI.2002.800574.

a known voltage on the boundary of Ω corresponds to the Dirichlet boundary condition

$$u(x,y) = f(x,y), \quad (x,y) \in \partial\Omega \tag{2}$$

where $\partial\Omega$ denotes the boundary of Ω, and knowledge of the resulting current density distribution on the boundary gives rise to the Neumann boundary condition

$$\gamma(x,y)\frac{\partial u}{\partial \nu}(x,y) = j(x,y) \tag{3}$$

where ν denotes the inward normal to $\partial\Omega$. The mapping which takes a given voltage distribution on the boundary to the resulting current density distribution on the boundary is referred to as the Dirichlet-to-Neumann or voltage-to-current map and is denoted by Λ_γ. Since the physical interpretation of Λ_γ is knowledge of the resulting current distributions on the boundary of Ω corresponding to all possible voltage distributions on the boundary, it can be viewed as our data.

III. The Reconstruction Algorithm

Nachman's uniqueness proof [25] for the 2-D inverse conductivity problem outlines a direct procedure for reconstructing the conductivity from knowledge of the Dirichlet-to-Neumann map. The idea behind the algorithm is to transform the conductivity equation to the Schrödinger equation and use the $\bar{\partial}$ method of inverse scattering to solve the resulting inverse problem. We remark that the $\bar{\partial}$ method is not a numerical technique, but rather a method of solution for certain inverse boundary value problems [5].

Let q be a bounded potential. Then, the change of variables $q = \gamma^{-1/2}\Delta\gamma^{1/2}$ and $\tilde{u} = \gamma^{1/2}u$ transforms the conductivity (1) to the Schrödinger equation

$$(-\Delta + q)\tilde{u} = 0 \text{ in } \Omega. \tag{4}$$

If one assumes that $\gamma = 1$ near the boundary of the region Ω, one can extend $\gamma = 1$ and $q = 0$ to the whole plane $\mathbb{R}^2$.

Note that if $q = 0$, the function $\tilde{u} = e^{ikz} = e^{i(k_1+ik_2)(x+iy)}$ satisfies $-\Delta\tilde{u} = 0$ in $\mathbb{R}^2$ where i denotes the complex number $\sqrt{-1}$, and we have introduced the complex parameter $k \neq 0$. Nachman shows [25] that the Schrödinger equation

$$(-\Delta + q)\psi(z,k) = 0 \quad z \in \mathbb{R}^2, \quad k \in \mathbb{C} \setminus 0 \tag{5}$$

has a unique solution $\psi(z,k)$ which is asymptotic to e^{ikz}. That is, when $|z|$ is large, $\psi(z,k)$ is approximately equal to e^{ikz} in a certain function space. The functions $\mu(z,k)$ defined by

$$\mu(z,k) := e^{-ikz}\psi(z,k)$$

hold the key to the reconstruction of the conductivity $\gamma(z)$ because one can show that

$$\lim_{k\to 0} \mu(z,k) = \gamma^{1/2}(z).$$

The $\bar{\partial}$ approach is used in determining μ from the voltage-to-current map, and taking the small k limit gives the conductivity directly at each point z in Ω.

A $\bar{\partial}$ equation is an equation of the form

$$\frac{\partial \mu}{\partial \bar{k}} = \Psi(k,\bar{k}) \quad z \in D$$

where D is a simply connected domain in $\mathbb{C}$ and the operator $\bar{\partial}$ is defined by

$$\bar{\partial} = \frac{\partial}{\partial \bar{k}} = \frac{1}{2}\left(\frac{\partial}{\partial k_1} + i\frac{\partial}{\partial k_2}\right).$$

The idea behind the $\bar{\partial}$ method is to apply the $\bar{\partial}$ operator to an integral equation that governs the solution of the scattering problem and derive a $\bar{\partial}$ equation that the solution satisfies. In the EIT problem, the function μ satisfies an integral equation analogous to the classical Lippmann–Schwinger equation, and applying the $\bar{\partial}$ operator to that equation yields the $\bar{\partial}$ equation

$$\frac{\partial}{\partial \bar{k}}\mu(z,k) = \frac{1}{4\pi\bar{k}}\mathbf{t}(k)e_{-k}(z)\overline{\mu(z,k)}, \quad k \in \mathbb{C}\setminus 0, \quad z \in \mathbb{R}^2. \tag{6}$$

Here, the functions $e_k(z)$ and $\mathbf{t}(k)$ are defined by

$$e_k(z) := e^{i(kz+\bar{k}\bar{z})}, \qquad \mathbf{t}(k) := \int_{\mathbb{R}^2} e_k(z)q(z)\mu(z,k)dz. \tag{7}$$

Note that $|e_k(z)| = 1$.

The function $\mathbf{t}$ is known as the scattering transform. Although it is not a physically measurable function, Nachman shows that it is related to the voltage-to-current data via the following integral equation:

$$\mathbf{t}(k) = \int_{\partial\Omega} e^{i\bar{k}\bar{z}}(\Lambda_\gamma - \Lambda_1)\psi(z,k)d\sigma(z). \tag{8}$$

Here, Λ_γ denotes the voltage-to-current map when Ω contains the conductivity distribution $\gamma(z)$, and Λ_1 denotes the voltage-to-current map when Ω contains a constant conductivity of 1.

Hence, the reconstruction method consists of two main steps

$$\Lambda_\gamma \xrightarrow{1} \mathbf{t} \xrightarrow{2} \gamma$$

1) determine the scattering transform $\mathbf{t}$ from the Dirichlet-to-Neumann map;
2) reconstruct γ using the $\bar{\partial}$ method.

IV. Numerical Techniques

A. Step 1: Determining the Scattering Transform $\mathbf{t}(k)$

In this paper, we study reconstructions of a numerically simulated phantom chest given an accurate representation of the scattering transform. For this goal, we omit Step 1 in the reconstruction algorithm and instead use the scattering transform computed from the definition (7). To accomplish this, we require an accurate representation of $\mu(x,k)$. This was obtained by numerically solving the Lippmann–Schwinger type equation for μ. See [24] for details.

Note that the Lippmann–Schwinger type equation does not make use of the measured data, but rather is an integral equation formulation of (4) and, thus, corresponds to the forward problem of determining μ from q. It is a subject of a future study to find a way to approximately compute $\mathbf{t}(k)$ from electrode measurements. Also note that it is not physically realistic to simply add noise to $\mathbf{t}(k)$ to simulate noise in the data. A correct simulation of noisy data would require adding noise to the simulated voltage-to-current map Λ_γ in (8) and then computing $\mathbf{t}(k)$ from that equation. In [24], this approach is taken for several examples of radially symmetric conductivities.

B. Step 2: Numerical Solution of the $\bar{\partial}$ Equation

Nachman shows that the solution of (6) satisfies the weakly singular Fredholm integral equation of the second kind

$$\mu(z,s) = 1 + \frac{1}{(2\pi)^2}\int_{\mathbb{R}^2} \frac{\mathbf{t}(k)}{(s-k)\bar{k}} e_{-z}(k)\overline{\mu(z,k)}dk_1dk_2 \quad (9)$$

for all $k \in \mathbb{C}\backslash 0$. Note that it is shown in [27] that for sufficiently smooth conductivities, $\mathbf{t}(k)/\bar{k}$ is bounded at $k = 0$ and the integrand in (9) approaches zero as $|k| \to \infty$. Thus, the integral over $\mathbb{R}^2$ can be approximated by an integral over a rectangle R. Also note that the integral is taken over the complex plane, so to solve (9) $\mu(x,s)$ is needed for all values of $s \in \mathbb{C} \setminus 0$. We solve (9) numerically using a 2-D adaptation of the method of product integrals presented in [2]. The idea of the method is to factor the integrand into its smooth part and its singular part and approximate the smooth part with a simple function, such as an interpolatory polynomial. The new integrand is then computed analytically where possible.

Given a sufficiently large rectangle R we first define a mesh $M = \{(u_j, v_i): i,j = 0,\ldots,N+1\}$ on the rectangle R in such a way that $k = 0$ is not a mesh point. We approximate the function $f(z,k) := (\mathbf{t}(k)/\bar{k})e_{-z}(k)\overline{\mu(z,k)}$ using bilinear interpolation, except on the mesh square Q_0 containing $k = 0$. On the square Q_0, we use the fact that $(\mathbf{t}(k)/\bar{k})|_{k=0} = 0$ and include a fifth interpolation point at the origin with $f(z,0) = 0$. This divides Q_0 into four triangles T_i, $i = 1$, 2, 3, and 4. On each triangle we approximate $f(z,k)$ by the plane through the two points on the corners of Q_0 and the origin. We denote the interpolant of $f(z,k)$ by $[f(z,k_1,k_2)]_{ji}$, where this notation represents the planar interpolant on T_i and the bilinear interpolant on all squares except Q_0.

On the outermost squares in the mesh M, which we will denote by $S := \{[u_j,u_{j+1}] \times [v_i,v_{i+1}]: j \in \{0,N-1\}$ or $i \in \{0,N-1\}\}$, we set $\mu \equiv 1$, using the fact that $\mu \sim 1$.

This leads to the discretized form of (9)

$$\mu(z,s) = g(z,s) + \frac{1}{4\pi^2}\sum_{j=1}^{N-1}\sum_{i=1}^{N-1}\int_{u_j}^{u_{j+1}}\int_{v_i}^{v_{i+1}} \frac{1}{s-k} \times [f(z,k_1,k_2)]_{ji}dk_1dk_2 \quad (10)$$

where

$$g(z,s) := 1 + \frac{1}{4\pi^2}\int_S \frac{1}{s-k}[f(z,k_1,k_2)]_{ji}dk_1dk_2. \quad (11)$$

To obtain a linear system, we choose s to be the nodes of the inner mesh elements $\{s = (u_j,v_i)\}_{j,i=1}^N$. Then, to form (10) and (11), the following integrals must be evaluated for $j,i = 0,\ldots,N$ and $s = (u_m,v_n)$, $m,n = 1,\ldots,N$

$$J_{\alpha\beta}^{ji}(s) := \int_{u_j}^{u_{j+1}}\int_{v_i}^{v_{i+1}} \frac{k_1^\alpha k_2^\beta}{(s-k)}dk_1dk_2, \quad \alpha,\beta \in \{0,1\}. \quad (12)$$

The factors of k in the numerator arise from the bilinear interpolant of f. On Q_0 we must evaluate

$$\int_{T_i} \frac{k_j}{s-k}dk_1dk_2, \quad j = 0,1, \quad i = 1,2,3,4. \quad (13)$$

When s lies on a corner of the mesh element over which we are integrating, an integrable singularity will be present in the integrand. When s does not coincide with a corner of the mesh element over which we are integrating, the above integrals are not singular, and they can be computed using a numerical quadrature method such as 2-D Gauss–Legendre quadrature. The singular integrals in (12) and (13) can be evaluated analytically. Note that there are 16 singular integrals in (12) and eight in (13). We omit their solutions for brevity.

Let $\mu_{ji}(z)$ denote $\mu(z,(u_j,v_i))$. Now by regrouping terms in (10), one can write

$$\mu_{ji}(z,s) = g_{ji}(z) + \frac{1}{4\pi^2}\sum_{j=1}^{N-1}\sum_{i=1}^{N-1} A^{ji}(z)\overline{\mu_{ji}(z)} \quad (14)$$

where $A^{ji}(z)$ is a linear combination of the $J_{\alpha\beta}^{ji}$s and the four integrals in (13). Thus, we have the linear system

$$\mathbf{I}\mu(z) - \mathbf{A}\bar{\mu}(z) = \mathbf{g}(z) \quad (15)$$

where $\mathbf{A}(z)$ is the N^2 by N^2 matrix $\mathbf{A}(z) = (A^{ji}(z))$ and $\mathbf{I}$ is the N^2 by N^2 identity matrix. This system can be solved by equating the real and imaginary parts to obtain two linear systems in real variables with two vectors of unknowns.

Note that the factors $J_\alpha^{ji}(s)$ in the matrix $\mathbf{A}$ are independent of z, so they need only be computed once and stored. Then in parallel, the matrix $\mathbf{A}$ is assembled and the resulting systems (15) are solved.

The solution of the system (15) results in a set of values of $\mu(z,k)$ for $k \in M$ and some discrete set of z values in Ω. Recall that the conductivity is given by

$$\gamma^{1/2}(z) = \lim_{k\to 0}\mu(z,k). \quad (16)$$

The value of $\mu(z,0)$ was approximated in this implementation using bicubic interpolation on the 16 values of $\mu(z,k)$ nearest $k = 0$ in the mesh M.

V. Numerical Example

We build a virtual chest phantom inside the unit disc $\Omega = B(0,1) \subset \mathbb{R}^2$. We choose elliptical domains to represent the heart and two lungs. The magnitudes of the conductivities are chosen to simulate a difference image of the chest during breath-holding when the heart is in systole and the reference image is during diastole. We make the assumptions that the detected conductivity changes are due to changes in blood volume, and our model heart holds a maximum of 200 ml of blood, while our model lungs have a resting volume of 2 l, one-third of which is tissue volume. If during systole the heart ejects a stroke volume of 100 ml which is distributed to the lungs, then the conductivity of the heart has decreased by a factor of two and the conductivity of the lungs has increased by 15%. In our virtual phantom, we simulate these relative changes by choosing a background conductivity of 1.0, the conductivity of the heart to be 0.5 and the conductivity of the lungs to be 1.2. Since Nachman's method is valid only for conductivities with two derivatives, we use a polynomial smoothing on the boundaries of the virtual organs. For a plot of the simulated conductivity, see Fig. 1.

The numerical approximation to the scattering transform $\mathbf{t}(k)$ was computed by the method in Section IV-A, and the $\bar{\partial}$ equation was solved by the method in Section IV-B using the uniform k-mesh $[-20,20]^2$ with meshsize $h \approx 1$. Note that this defines the rectangle R in Section IV-B. For this example, the

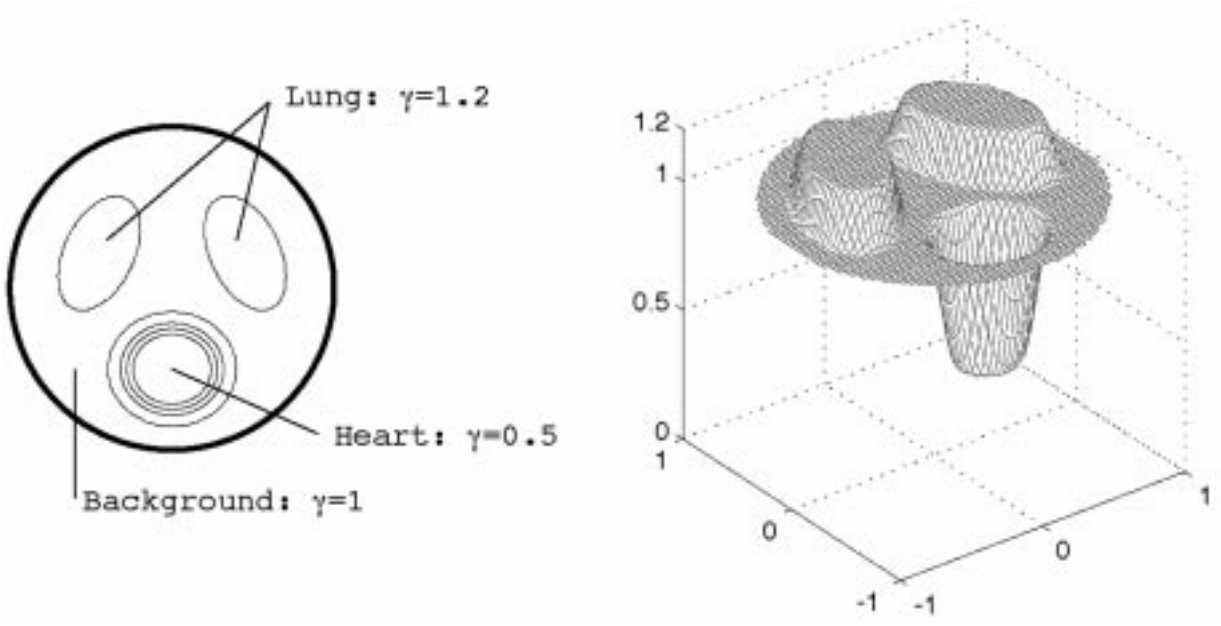

(a) (b)

Fig. 1. (a) Contour plot and (b) 3-D plot of the actual conductivity $\gamma(x)$.

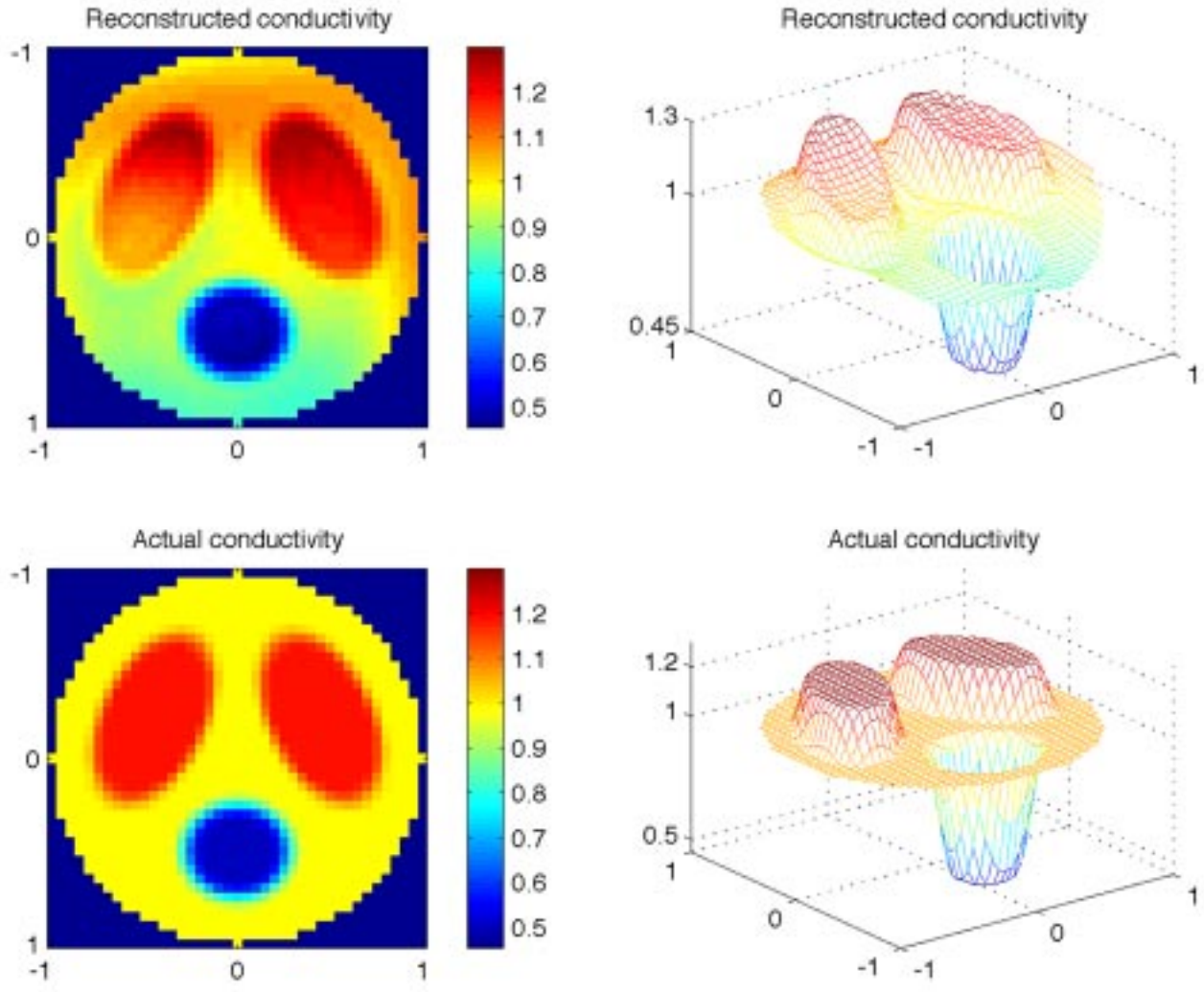

Fig. 2. Plots of the actual and reconstructed conductivities for the virtual phantom chest.

scattering transform decays slowly, and this choice of mesh ensures that $|\mathbf{t}(k)/\bar{k}| < 0.1$ for $|k| = 20$. A study of the effects of truncating tbe scattering transform at radius r on the reconstructions is found in [24] where it is shown that the reconstructions corresponding to such truncations will converge to the correct conductivity, and several numerical examples are provided. However, a quantitative study of the effect of the size of the rectangle R on the reconstruction remains for future work. For each x value, the value of $\gamma^{1/2}(x)$ was obtained by using bicubic interpolation on the 16 values of the real part of $\mu(x,k)$ nearest $k = 0$. Plots of the reconstruction and the actual conductivity were generated in Matlab using the commands imagesc for the surface plots and mesh for the three-dimensional (3-D) plots. They are plotted on the same scale and are found in Fig. 2. The reconstructed conductivity has a maximum value of 1.2996, which is found in the lung region, and a minimum value of 0.4535, which is found in the heart region. These correspond to relative errors of 8.3% and 9.3%, respectively.

VI. Conclusion

The locations of the virtual heart and lungs were well approximated by the reconstruction. The actual conductivity values were also recovered to within 10% accuracy. It remains to test the algorithm on noisy voltage-to-current maps, as was done in [24], for physically relevant simulations such as our virtual phantom chest. It also remains to test the algorithm on measured data. Both of these steps will require some further development on the algorithm and its implementation than currently exists. Nevertheless, the reconstructions from an accurate scattering transform give encouraging results for the ability of the method to accurately reconstruct conductivity values in the chest.

Acknowledgment

The authors would like to thank J. Newell for his help in designing the test problem.

References

[1] A. Allers and F. Santosa, "Stability and resolution analysis of a linearized problem in electrical impedance tomography," *Inverse Prob.*, vol. 7, pp. 515–533, 1991.

[2] K. Atkinson, *An Introduction to Numerical Analysis*, 2nd ed. New York: Wiley, 1989.

[3] D. C. Barber and B. H. Brown, "Applied potential tomography," *J. Phys. E. Sci. Instrum.*, vol. 17, pp. 723–733, 1984.

[4] ——, "Progress in electrical impedance tomography," in *Inverse Problems in Partial Differential Equations*. Philadelphia, PA: SIAM, 1990.

[5] R. Beals and R. R. Coifman, "The d-bar approach to inverse scattering and nonlinear evolution equations," *Physica*, vol. 18, pp. 242–249, 1986.

[6] C. Berenstein and E. C. Tarabusi, "Inversion formulas for the k-dimensional Radon transform in real hyperbolic spaces," *Duke Math. J.*, vol. 62, pp. 1–19, 1991.

[7] R. Blue, "Real-time three-dimensional electrical impedance tomography," Ph.D. dissertation, Rensselaer Polytechnic Inst., Troy, NY, 1997.

[8] L. Borcea, "Nonlinear multigrid for imaging electrical conductivity and permittivity at low frequency," *Inverse Prob.*, vol. 17, no. 2, pp. 329–359, 2001, Preprint.

[9] L. Borcea, J. G. Berryman, and G. Papanicolaou, "High contrast impedance tomography," *Inverse Prob.*, vol. 12, pp. 835–858, 1996.

[10] A. P. Calderón, "On an inverse boundary value problem ," in *Seminar on Numerical Analysis and its Applications to Continuum Physics*. Rio de Janeiro, Brazil: Soc. Brasileira de Matemàtica, 1980, pp. 65–73.

[11] M. Cheney, D. Isaacson, and E. L. Isaacson, "Exact solutions to a linearized inverse boundary value problem," *Inverse Prob.*, vol. 6, pp. 923–934, 1990.

[12] M. Cheney, D. Isaacson, J. C. Newell, J. Goble, and S. Simske, "Noser: And algorithm for solving the inverse conductivity problem," *Int. J. Imag. Syst. Technol.*, vol. 2, pp. 66–75, 1990.

[13] D. C. Dobson, "Convergence of a reconstruction method for the inverse conductivity problem," *SIAM J. Appl. Math.*, vol. 52, no. 2, pp. 442–458, 1992.

[14] D. C. Dobson and F. Santosa, "An image-enhancement technique for electrical impedance tomography," *Inverse Prob.*, vol. 10, pp. 317–334, 1994.

[15] O. Dorn, H. Berteta-Aguirre, J. G. Berryman, and G. Papanicolaou, "A nonlinear inversion method for 3D-electromagnetic imaging using adjoint fields," *Inverse Prob.*, vol. 15, pp. 1523–1558, 1999.

[16] D. Isaacson and M. Cheney, "Effects of measurement precision and finite numbers of electrodes on linear impedance imaging algorithms," *SIAM J. Appl. Math.*, vol. 15, pp. 1705–1731, 1991.

[17] J. Kaipio, V. Kolehmainen, E. Somersalo, and M. Vauhkonen, "Statistical inversion and monte carlo sampling methods in electrical impedance tomography," *Inverse Prob.*, vol. 16, pp. 1487–1522, 2000.

[18] J. S. Kallman and J. G. Berryman, "Weighted least-squares criteria for electrical impedance tomography," *IEEE Trans. Med. Imag.*, vol. 11, pp. 284–292, June 1992.

[19] M. Klibanov, "A Newton-Kantorovich method for impedance computed tomography," , Preprint.

[20] R. V. Kohn and A. McKenney, "Numerical implementation of a variational method for electrical impedance imaging," *Inverse Prob.*, vol. 9, pp. 389–414, 1990.

[21] R. V. Kohn and M. Vogelius, "Relaxation of a variational method for impedance computed tomography," *Commun. Pure Appl. Math.*, vol. 40, pp. 745–777, 1987.

[22] ——, "A reconstruction algorithm for electrical impedance tomography data collected on rectangular electrode arrays," *IEEE Trans. Biomed. Eng.*, vol. 49, pp. 1379–1386, Nov. 1999.

[23] ——, "Reconstruction of conductivity changes due to ventilation and perfusion from EIT data collected on a rectangular electrode array," *Physiol. Meas.*, vol. 22, pp. 97–106, 2001.

[24] J. L. Mueller and S. Siltanen, "Direct reconstructions of conductivities from boundary measurements," *SIAM J. Sci. Comput.*, 2001, Preprint..

[25] A. I. Nachman, "Global uniqueness for a two-dimensional inverse boundary value problem," *Ann. Math.*, vol. 143, pp. 71–96, 1996.

[26] F. Santosa and M. Vogelius, "A backprojection algorithm for electrical impedance imaging," *SIAM J. Appl. Math.*, vol. 50, pp. 216–243, 1990.

[27] S. Siltanen, J. Mueller, and D. Isaacson, "An implementation of the reconstruction algorithm of A. Nachman for the 2-D inverse conductivity problem," *Inverse Prob.*, vol. 16, pp. 681–699, 2000.

[28] ——, "Errata: An implementation of the reconstruction algorithm of A. Nachman for the 2-D inverse conductivity problem," *Inverse Prob.*, vol. 17, pp. 1561–1563, 2001.

[29] ——, "Reconstruction of high contrast 2-D conductivites by the algorithm of A. Nachman," in *Proc. 2000 Conf. Radon Transforms and Tomography*, Quinto *et al.*, Eds., 2001, pp. 241–254.

[30] E. Somersalo, M. Cheney, D. Isaacson, and E. Isaacson, "Layer stripping: A direct numerical method for impedance imaging," *Inverse Prob.*, vol. 7, pp. 899–926, 1991.

[31] A. J. Suroviec, S. S. Stuchly, J. R. Barr, and A. Swarup, "Dielectric properties of breast carcinoma and the surrounding tissues," *IEEE Trans. Biomed. Eng.*, vol. 35, pp. 257–263, Apr. 1988.

[32] A. Swarup, S. S. Stuchly, and A. Surowiec, "Dielectric properties of mouse mca1 fibrosarcoma at different stages of development," *Bioelectromagnetics*, vol. 12, no. 1, p. 108, 1991.

[33] J. Sylvester, "A convergent layer stripping algorithm for the radially symmetric impedance tomography problem," *Commun. Partial Differential Equations*, vol. 17, pp. 1955–1994, 1992.

[34] A. Wexler, B. Fry, and M. Neuman, "Impedance computed tomography algorithm and system," *Appl. Opt.*, vol. 24, pp. 3982–3985, 1985.

[35] T. J. Yorkey, J. G. Webster, and W. J. Tompkins, "Comparing reconstruction algorithms for electrical impedance tomography," *IEEE Trans. Biomed. Eng.*, vol. BME-34, pp. 843–852, 1987.